Angular distribution of debris from CO_2 and YAG laser-produced tin plasmas

D. Campos, R. W. Coons, M. D. Fields, M. Crank, S. S. Harilal, and A. Hassanein

School of Nuclear Engineering, and Center for Materials Under Extreme Environment
Purdue University, West Lafayette, Indiana, 47907, USA

ABSTRACT

We investigated the angular dependence of atomic and ionic debris from CO_2 and YAG laser-produced tin plasmas. Several diagnostic techniques were employed for this study including a Faraday cup, witness plates and subsequent x-ray photoelectron spectroscopic analysis, optical emission spectroscopy etc. It was found that the debris emission from the Nd:YAG laser-produced plasmas fell sharply from the target normal. In contrast, the debris emission from the CO_2 laser-produced plasmas was almost constant at short angles from the target normal. Our results also indicated that the plasma produced by the CO_2 laser emitted less atomic and ionic debris compared to a plasma produced by Nd:YAG laser.

I. INTRODUCTION

Optical lithography is rapidly approaching its physical limitations as the semiconductor industry continues to call for smaller features for technological advances. For the industry to keep up with Moore's law, a reliable, commercially viable extreme ultraviolet lithography (EUVL) light source at 13.5 must be developed. The selection of 13.5 nm radiation relies on the availability of multilayer mirrors (MLMs) which reflect a 2% bandwidth centered at 13.5 nm (commonly called in-band radiation). Spitzer et al [1] found that tin targets irradiated by a Nd:YAG laser provided a high conversion efficiency (CE) from laser power to in-band EUV radiation around 13.5 nm thus establishing laser produced plasmas (LPPs) as a leading candidate for an EUVL source. For a plasma to possess high CE, not only must it have an electron temperature of ~30-40 eV, but also it must not be optically thick which prevents release of EUV photons. Many studies have shown that the EUV emission characteristics of LPP depend strongly on a number of factors including target geometry [2], target material [3], laser spot size [4, 5], laser wavelength [3, 6, 7], etc.

A suitable EUV source requires high CE as well as efficient mitigation of debris. The MLMs are highly susceptible to damage caused by energetic ions, neutral atomic debris as well as molten droplets of ablated material. The debris can cause reflectivity losses through vapor deposition of monolayers of target material as well as damage produced by incident ions. Furthermore, heat loading from out-of-band radiation can cause significant distortion of the geometry of the MLM introducing another significant source of reflectivity loss [8]. Therefore, spectral purity is another requirement for the development of an effective EUV source. Initially, only Nd:YAG excitation was explored thoroughly for EUVL source development, but later it was found that excitation from a CO_2 laser provides a comparable CE to Nd:YAG laser excitation thus establishing CO_2 LPPs as a worthy candidate for EUVL [7]. Moreover, it was found that the CO_2 LPP provides a narrower unresolved transmission array (UTA) around 13.5 nm due to its lower opacity [9].

In this report, we detail the differences in debris profiles from CO_2 and Nd:YAG LPPs including an angularly-resolved comparative study. The purpose of this experiment is to explore potential advantages of using CO_2 LPPs versus Nd:YAG LPPs for EUVL source development. To this end, we employed witness plates, X-ray photoelectron spectroscopy (XPS), Faraday cup ion fluence analysis and optical emission spectroscopy (OES) as well as EUV pinhole imaging. It was found that the Nd:YAG LPP emitted a

Extreme Ultraviolet (EUV) Lithography, edited by Bruno M. La Fontaine, Proc. of SPIE Vol. 7636,
763612 · © 2010 SPIE · CCC code: 0277-786X/10/$18 · doi: 10.1117/12.848333

significantly greater amount of ionic debris per laser pulse than the CO_2 LPP. A significant difference in the angular distribution of atomic and ionic debris was also observed.

II. EXPERIMENTAL SETUP

A schematic of the experimental setup is given in figure 1. For producing plasmas, the radiation from a transversely excited atmospheric CO_2 laser (10.6 μm 30 ns FWHM) and from a Nd:YAG laser (1.06 μm 8 ns FWHM) was focused onto a planar tin slab mounted on a servo-motor controlled XYZ translation stage giving high precision of movement in all 3 directions. The mirror used to divert the 1.06 μm radiation to the chamber was placed on a flip mount for easy removal from the 10.6 μm beam's optical path. A simple plasma shutter device was placed in the beam path of the CO_2 laser to clip the nitrogen tail of the pulses [10]. For ion analysis, the charge collecting surface of the Faraday cup was placed 17.2 cm away from the target at various angles from the target normal. The FC was biased using a DC voltage power supply to an optimized voltage of -31 V to deflect incoming electrons as well as for minimizing signal noise.

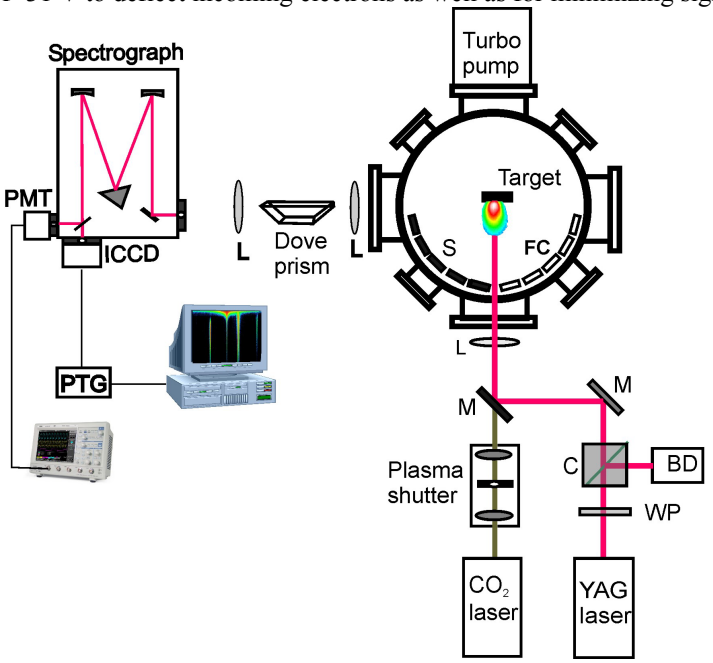

Figure 1: The schematic of the experimental set up. (WP, waveplate; C, polarizing cube; BD, beam dump; M, mirror; L, lens; S, substrate; FC, Faraday cup; PMT, photomultiplier tube; ICCD, intensified charge-coupled device; PTG, programmable timing generator)

To conduct the studies of atomic debris, silicon witness-plates were placed at 13 cm away from the target again at identical angles from the target normal. For this experiment, two sets of wafers were placed around the chamber symmetrically about the laser path to provide more data for averaging. These wafers were then transported to IMPACT for XPS analysis; a comprehensive description of this facility is located elsewhere [11]. A Mg Kα source emitting at 1254 eV was used for the XPS studies. The atomic fractions are calculated based on the integrated area under the peaks in the spectra using CasaXPS. These areas are weighted according to the relative intensities of the spectral lines the details of which can be found elsewhere [12].

We employed 2D spectral imaging using a 0.5 m spectrograph equipped with an intensified charge-coupled device (ICCD) for characterizing the plasma. The spectrograph was equipped with three gratings of 150 grooves/mm, 600 grooves/mm, and 1800 grooves/mm, with effective dispersions of 12.6 nm/mm, 3.1 nm/mm, and 1.03 nm/mm respectively. A dove prism was inserted in the optical path of the image to rotate it 90º; this was done so that the image would expand axially down the spectrograph slit instead of

transversely across it. In this way, it was possible to achieve very high spatial resolution for density measurements, and it was possible to estimate the plasma density within several hundred μm of the target [13].

III. RESULTS AND DISCUSSION

In addition to requiring high CE, a viable LPP EUVL source must cause minimum damage to the MLMs. This damage results from the ions and neutrals emitted from the plasma plume and heat loading of the mirror caused by out of band emission. Several methods of debris mitigation have been investigated such as magnetic fields [14], ambient gases [15], and mass-limited targets [16]; however, for these protective schemes to succeed, it is essential to develop a thorough understanding of the ionic, atomic, and particulate emissions from LPPs. The chosen power densities for the experiments were 2×10^{11} W/cm^2 and 6×10^9 W/cm^2 respectively for Nd:YAG and CO_2 laser excitation. These laser intensities were chosen because they represent the optimum power densities to maximize CE [5, 17]. Typical EUV emission images were obtained using the pinhole camera and are given in figure 2. The camera integrates the EUV emission in the 7-15 nm spectral range; hence it captures approximately the complete unresolved transmission array (UTA). The emission features show clear differences; namely, that the Nd:YAG LPP exhibits a conical emission where as the CO_2 displays a hemispherical expansion.

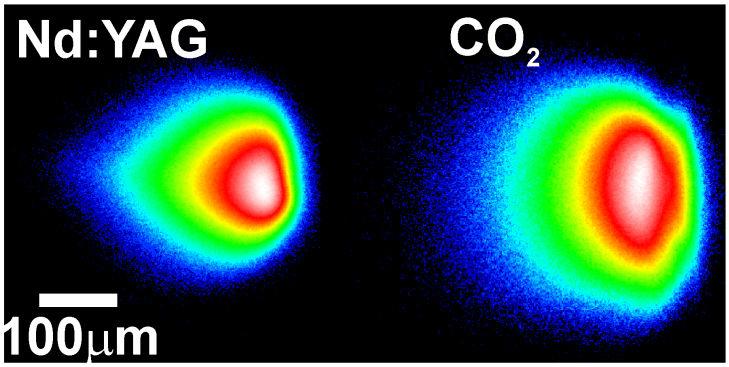

Figure 2: The EUV pinhole images obtained from Nd:YAG and CO_2 produced Sn plasmas. A combination of 50 μm pinhole and a Zr-filter were used for obtaining these images. The Nd:YAG laser spot size was 100 μm and the CO_2 laser spot size was 225 μm.

The FC ion analysis garnered very interesting results. Typical ion profiles obtained using the FC are given for CO_2 and Nd:YAG LPPs along with their kinetic energy profiles. It can be seen in figure 3 that the ion fluence was significantly higher for the Nd:YAG LPP compared to the CO_2 LPP due to the narrower ion profiles obtained for the CO_2 LPP. However, the kinetic distribution of CO_2 LPP is shifted to the higher energy side (figure 3 inset). We constructed an angular distribution of the ionic debris from both excitation wavelengths by plotting the integrated area of the ion profiles against the angle with respect to target normal. This plot is given in figure 4. The wavelength effects on ion fluence are intriguing because of the sharp contrast in the angular distributions of the ionic debris. The ion flux from Nd:YAG LPP falls off rapidly away from the target normal whereas the CO_2 debris does not fall off sharply until farther away from the target normal.

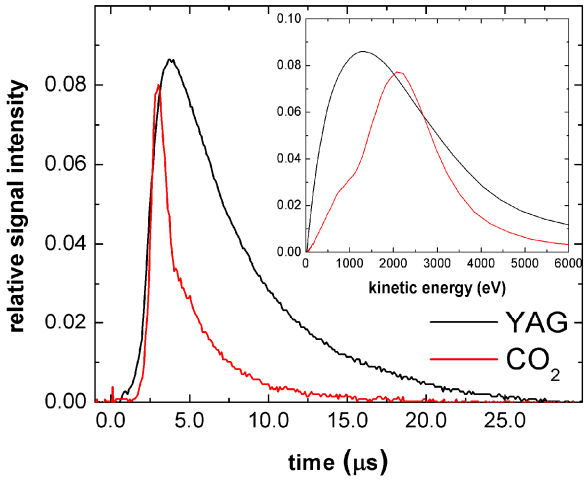

Figure 3: Typical ion time of flight signals measured using the FC. The kinetic energy profiles are given in the inset and calculated using the velocities obtained from the raw data. These data were obtained at 12° from the target normal.

It is known that atomic particles also cause severe damage to the MLMs through deposition. Hence, we investigated the angular distribution of atomic debris using witness plates. Analysis of the witness plates was carried out using XPS which provides atomic fraction data. A representative XPS spectrum is given in figure 5. Along with Sn photoelectron peaks, impurity peaks (C1s & O1s) and substrate peaks (Si 2s and 2p) were also seen in the core electron spectra. The smaller peaks immediately following the O 1s peak and the C 1s peaks are satellite peaks and should be disregarded when attempting to obtain elemental information. The strength of the oxygen and carbon peaks is due to their extremely high relative sensitivity factors as given in the previous reference [12]. Using the data from the other angles we were able to construct an angular atomic fraction profile which is given in figure 6. This figure clearly indicates that atomic debris is significantly higher from Nd:YAG LPPs versus CO_2 LPPs. The angular distribution of atomic emission from Nd:YAG LPPs decreases rapidly away from target normal similar to the ion flux given in figure 4.

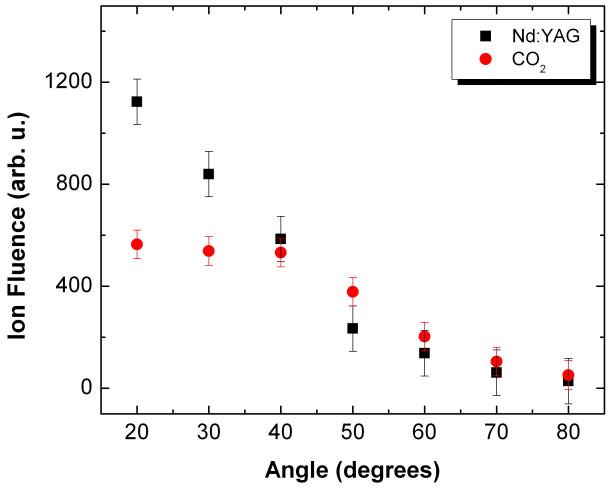

Figure 4: The angular distribution of ion flux obtained from FC data. For this measurement FC was positioned at 17 cm from the laser focal spot.

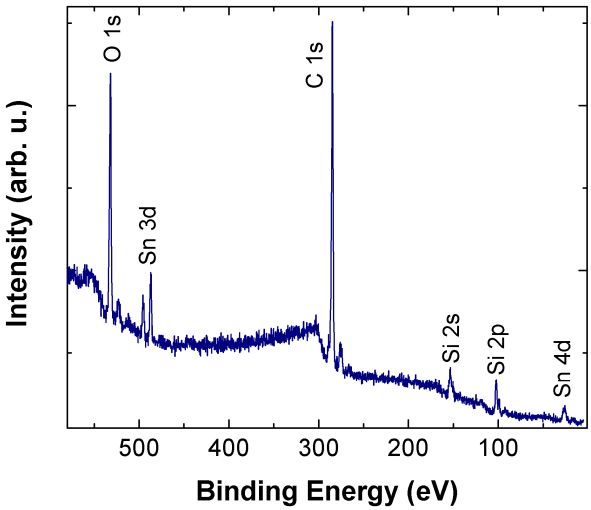

Figure 5: A representative XPS spectrum from 2000 CO_2 laser pulses. The oxygen and carbon peaks as well as their respective satellite peaks can be safely neglected for the purpose of calculating the relative fractions of tin and silicon.

To better understand the wavelength effects on ion and atomic flux, we estimated basic plume parameters using spectroscopic means. The recorded spectra showed a strong presence of excited neutrals and singly-ionized Sn species in the visible emission spectral region. Using Stark Broadening measurements [18], we estimated the densities of the plasmas at various spatial locations from the target surface. Typical Stark broadened 2D spectral images of Sn^+ at 645.4 nm are given in figure 7. The spectral images clearly show higher spatial extension for the visible emission from the Nd:YAG LPP. The estimated values of electron density at 225 μm away from the target for Nd:YAG and CO_2 produced plasmas are 7.2×10^{17} cm^{-3} and 2.7×10^{17} cm^{-3} respectively and these values decay to 1.0×10^{17} cm^{-3} and 0.29×10^{17} cm^{-3} at 1 mm from the target. It should be mentioned that the above given values are time-integrated over 2 μs starting from onset of plasma formation. Interferometry studies [5, 19] showed that the plasma reached the critical densities of the excitation beams (~10^{21} cm^{-3} for 1.06 μm and ~10^{19} cm^{-3} for 10.6 μm) during peaks of the respective laser pulses. These data illuminate a key difference between CO_2 and Nd:YAG LPPs.

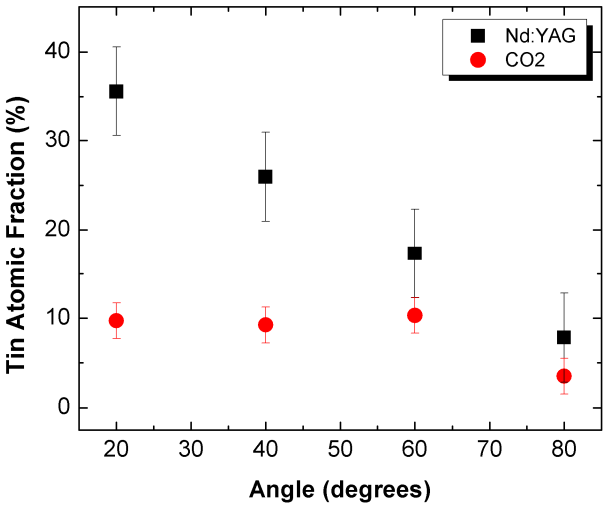

Figure 6: The atomic fractions of Nd:YAG and CO_2 debris from XPS analysis are given in this figure. The atomic fractions for CO_2 were divided by 2.5 because it was fired 2.5 more times (1750 shots) than the Nd:YAG (700 shots) for obtaining the results.

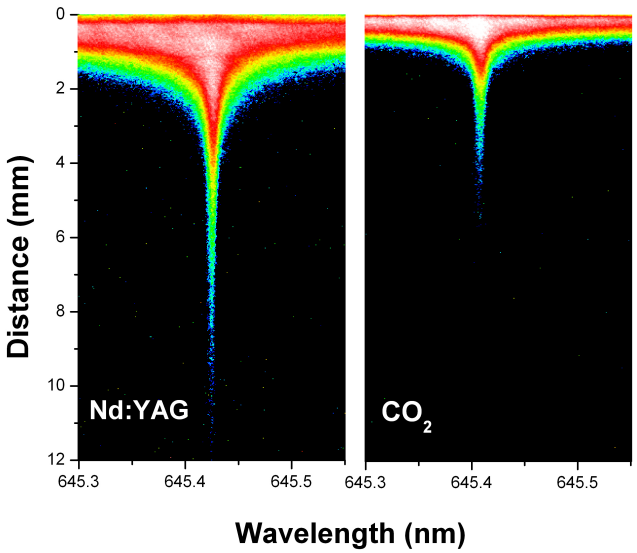

Figure 7: Typical Stark broadened profiles of Sn^+ obtained at 645.4 nm using 2D spectral imaging

The greater flux of atomic and ionic debris emitted by the Nd:YAG LPP in comparison with CO_2 plasma is caused by the disparity in initial densities of the plasmas. A major source of lower-charged ions and neutrals in a LPP, especially at extended regions and at later times, can be the result of collisional three-body recombination. The relation between three-body recombination rate and the density of the plasma is given by [20]

$$R_c \alpha Z^3 \ln\sqrt{Z^2+1}\; T_e^{-9/2} n_e^2 n_i \qquad (1)$$

where Z is the charge state, T_e is the electron temperature and n_e and n_i are the electron and ion densities respectively. Equation 1 shows that three-body recombination has an n_e^2 dependence and the higher density in the case of the Nd:YAG LPP may indeed fuel a higher rate of three-body recombination both near to and far away from the target. Hence, one can expect larger spatial extension of the various emitting species (as seen in figure 7) in the visible region for the Nd:YAG LPP. More experimental work is required to verify this interpretation.

Although the CO_2 LPP ions have narrower temporal profiles, they are shifted to the higher energy side in comparison with YAG LPP ion profiles. The lower rate of three-body recombination preserves the higher charge-states of ions emitted from the CO_2 LPP leading to a narrower kinetic energy distribution. It should be remembered that a FC signal contains all charge-states of ions emanating from the plasma. The velocities of ions emitted from LPPs are governed by space-charge effects created by electrons that leave the target at extremely high velocity and drag the positively-charged ions in their wake. It is also known that because of space-charge effects highly charged ions move much faster. This may explain the upward shift in kinetic energy for the CO_2 LPP.

We also believe that the difference in initial densities of the plasma may play a major role in obtaining the contrasting angular profiles of atomic and ionic debris. It is reported that the angular distribution of ionic debris emission is proportional to a $\sim\cos^n(\theta)$ function where n depends on the charge state and θ is the angle from the target normal [21]. The angular dependence of ionic emission from the Nd:YAG LPP is found to follow a first-order $\cos^n$ function. As the recombination processes occur, the ionic angular spread is expected to increase; however, the plasma ions continue to propagate in a generally forward direction. This results in significantly lower ion and atomic flux farther away from the target normal. For the CO_2 LPP, the low initial density results not only in the production of significantly less ions, but also allows more the highly-charged ions to escape from the recombination effects. This results in the production of significantly less neutral debris and thus, the lower amount of deposition on the witness plates.

Finally, the difference in initial densities and resultant disparity in the rates of recombination is what causes the marked difference in EUV emission profiles for the Nd:YAG and CO_2 LPPs. As shown in figure 2, the EUV image obtained from the Nd:YAG LPP shows a conical emission where as the CO_2 LPP shows a hemispherical expansion. It is clear from figure 2 that the aspect ratio of the Nd:YAG LPP is considerably higher than the CO_2 LPP. The major species that contribute to in-band emission are Sn^{9+} - Sn^{13+}, and lower-charged ions contribute to the UTA in the longer wavelength side of the out-of-band region [9]. It was previously noticed that the UTA of the CO_2 LPP was spectrally narrower compared to the Nd:YAG plasma [5, 16]. The emission from the extended region of cone in a YAG LPP results from the presence of lower-charged ions contributed by enhanced three-body recombination.

IV. CONCLUSIONS

We compared the angular distribution of atomic and ionic emission from Sn plasmas produced by Nd:YAG and CO_2 lasers. We observed a large disparity in both the amount of debris emission from the plasmas, and also the angular distributions of the various debris species. The forward-centric angular distribution of the Nd:YAG LPP atomic and ionic debris is due to the significantly higher rate of three-body recombination and thus the enhanced production of lower-charged ions and neutral species. The lower density of the CO_2 LPP leads to a smaller quantity overall ionic debris and due to the lower rate of three-body recombination significantly less neutral debris. While the kinetic energy distribution is shifted to higher energy for the CO_2 LPP, the distribution itself is much narrower, again, due preservation of highly-charged ionic species and may be due to a significantly lower recombination rate. Finally, this high rate of three-body recombination present in the Nd:YAG LPP likely is the cause of its further spatial extension of both visible and EUV emission.

ACKNOWLEDGEMENTS

This work was partially funded by the College of Engineering, Purdue University.

REFERENCES

[1] R. C. Spitzer, R. L. Kauffman, T. Orzechowski *et al.*, "Soft X-ray production from laser produced plasmas for lithography applications," Journal of Vacuum Science & Technology B, 11(6), 2986-2989 (1993).

[2] Y. Ueno, G. Soumagne, A. Sumitani *et al.*, "Enhancement of extreme ultraviolet emission from a CO2 laser-produced Sn plasma using a cavity target," Applied Physics Letters, 91(23), 3 (2007).

[3] A. Nagano, T. Mochizuki, S. Miyamoto *et al.*, "Laser wavelength dependence of extreme ultraviolet light and particle emissions from laser-produced lithium plasmas," Applied Physics Letters, 93(9), (2008).

[4] S. S. Harilal, "Influence of spot size on propagation dynamics of laser-produced Sn plasma," Journal of Applied Physics, 103, 123306 (2007).

[5] S. S. Harilal, R. W. Coons, P. Hough *et al.*, "Influence of spot size on extreme ultraviolet efficiency of laser-produced Sn plasmas," Applied Physics Letters, 95, 221501 (2009).

[6] A. Takahashi, D. Nakamura, K. Tamaru *et al.*, "Emission characteristics of debris from CO2 and Nd : YAG laser-produced tin plasmas for extreme ultraviolet lithography light source," Applied Physics B-Lasers and Optics, 92(1), 73-77 (2008).

[7] H. Tanaka, A. Matsumoto, K. Akinaga *et al.*, "Comparative study on emission characteristics of extreme ultraviolet radiation from CO2 and Nd : YAG laser-produced tin plasmas," Applied Physics Letters, 87(4), 3 (2005).

[8] T. Feigl, S. Yulin, T. Kuhlmann *et al.*, "Damage resistant and low stress EUV multilayer mirrors," Japanese Journal of Applied Physics Part 1-Regular Papers Short Notes & Review Papers, 41(6B), 4082-4085 (2002).

[9] J. White, P. Dunne, P. Hayden *et al.*, "Optimizing 13.5 nm laser-produced tin plasma emission as a function of laser wavelength," Applied Physics Letters, 90(18), 181502 (2007).

[10] N. Hurst, and S. S. Harilal, "Pulse shaping of transversely excited atmospheric CO2 laser using a simple plasma shutter," Review of Scientific Instrumentation, 80, 035101 (2009).

[11] J. P. Allain, M. Nieto, M. R. Hendricks *et al.*, "IMPACT: A facility to study the interaction of low-energy intense particle beams with dynamic heterogeneous surfaces," Review of Scientific Instruments, 78(11), (2007).

[12] M. P. Seah, [Quantification in AES and XPS] The Scottish Universities Summer School in Physics, Great Yarmouth, Norfolk, 1 (1993).
[13] J. Siegel, G. Epurescu, A. Perea *et al.*, "Temporally and spectrally resolved imaging of laser-induced plasmas," Optics Letters, 29(19), 2228-2230 (2004).
[14] S. S. Harilal, B. O'Shay, Y. Tao *et al.*, "Ion debris mitigation from tin plasma using ambient gas, magnetic field and combined effects," Applied Physics B-Lasers and Optics, 86(3), 547-553 (2007).
[15] S. S. Harilal, B. O'Shay, Y. Z. Tao *et al.*, "Ambient gas effects on the dynamics of laser-produced tin plume expansion," Journal of Applied Physics, 99(8), (2006).
[16] S. S. Harilal, B. O'Shay, M. S. Tillack *et al.*, "Spectral control of emissions from tin doped targets for extreme ultraviolet lithography," Journal of Physics D-Applied Physics, 39(3), 484-487 (2006).
[17] A. Hassanein, V. Sizyuk, T. Sizyuk *et al.*, "Effects of Plasma Spatial Profile on Conversion efficiency of Laser-Produced Plasma Sources for EUV lithography," J. Micro/Nanolith. MEMS MOEMS, 8(4), 041503 (2009).
[18] S. S. Harilal, B. O'Shay, M. S. Tillack *et al.*, "Spectroscopic Characterization of laser produced tin plasma," Journal of Applied Physics, 98(1), 013306 (2005).
[19] Y. Tao, M. S. Tillack, S. S. Harilal *et al.*, "Investigations on the interaction of a laser pulse with a preformed Gaussian Sn plume for an extreme ultraviolet lithography source," Journal of Applied Physics, 101, 023305 (2007).
[20] P. T. Rumsby, and J. W. M. Paul, "Temperature and density of an expanding laser-produced plasma," Plasma Physics and Controlled Fusion, 16(3), 247-260 (1974).
[21] A. Thum-Jager, and K. Rohr, "Angular emission distributions of neutrals and ions in laser ablated particle beams," Journal of Physics D-Applied Physics, 32, 2827-2831 (1999).